Pages: 75-87 / Vol. 18 ./ Issue 2 / Summer- Fall 2025

Journal of Aerospace Science and Technology

Journal Homepage: https://jast.ias.ir

Original Research Article

Numerical Study of Flow Pattern on A Diamond Wing-Body Equipped With LEX At Low Angles of Attack

Mohammad Reza Hashemi[1], Seyyed Majid Malek Jafarian[2]*, and Mojtaba Dehghan Manshadi[3]

1. Department of Mechanics, University of Birjand, Birjand, Iran
2. Department of Mechanical and Aerospace Engineering, MUT, Shahinshahr 3898, Iran

ARTICLE INFO

Received: 16 August 2024
Revised: 18 May 2025
Accepted: 31 May 2025
Available online: 07 July 2025

KEYWORDS:

Diamond wing-body
LEV
Dual-vortex structure
Flow field
CFD

ABSTRACT

In this research, the characteristics of the flow field around the diamond wing equipped with LEX have been studied using CFD. Investigations carried out at low angles of attack have included 5, 10, and 15 degrees, and Re= 2.16×105 based on the model length. An investigation of the vortical flow of the diamond wing can help identify the flow field characteristics and the phenomenon of vortex breakdown. The results indicated the presence of the LEV at the angle of attack of 5 degrees and for the cross-section close to the wing apex. The pressure coefficient showed that there are two low-pressure areas inside the vortex, which reveals a dual-vortex structure. Close to the center of the vortex, the amount of vorticity increased. Increasing the angle of attack has led to expanding the vortex core, which has finally created the conditions for the existence of secondary and third vortices. The third vortex rotates opposite the direction of the secondary vortex and in the same direction as the LEV. This subject, observed rarely on delta wings, leads to increased circulation and stability of the diamond wing.

DOI:
https://doi.org/10.22034/jast.2025.473495.1204

1 INTRODUCTION

In recent decades, flying wings and Blended wing body (BWB) aircraft have received special attention from the point of view of aerodynamic designers due to their special characteristics [1]. Diamond, lambda, double delta, and simple delta wings (with low leading-edge sweep-back angle) are used in the wing design of such aircraft [2]. Highly BWB designs are commonly used to achieve stealthy and agile attributes mainly due to the stealth requirements and their mission [3] [4]. The aerodynamic features of a diamond wing are almost similar to those of a delta wing with a low leading-edge sweep-back angle. At low and moderate angles of attack, the flow field formed on the delta wing includes separating the boundary layer at the leading-edge and forming a coherent leading-edge vortex (LEV) [5]. Many studies have been performed in the past. All of them have

* Corresponding Author's Email: mmjafarian@birjand.ac.ir

Print ISSN:1735-2134 Online ISSN: 2345-3648

confirmed the existence of a vortex with a coherent core on the delta wing at low and high Reynolds numbers, which can be attributed to the works of Muir et al. [6], Ol and Gharib [7], Butler [8], Werner et al. [9] and Kumar et al. [10]. Also, because of the LEVs, delta wings can reach a greater stall angle of attack and generate higher lift than other wing platforms [11]. At high angles of attack, due to the interaction between the LEV and the boundary layer, it is possible to form a secondary vortex (SV). These vortices have a significant axial velocity in the center of the core. Therefore, the negative pressure created in the span-wise direction of the wing has increased. This issue indicates a higher pressure difference between the lower and upper surfaces of the wing. As a result, the delta wings' stall is postponed to higher angles of attack and will have maneuverability [12]. At a particular angle of attack, the vortex flow on the wing is no longer detectable. This phenomenon is called vortex collapse or breakdown [13]. The most significant characteristics of vortex breakdown are the axial velocity reduction and the vortex core augmentation. As a consequence, the wake-like flow spreads over and downstream of the wing [14]. With an increment of the angle of attack, the location of the breakdown shifts upstream and close to the wing apex. If the breakdown reaches exactly the wing apex, the flow on the wing is completely separated, and a full stall has occurred [15]. In this case, the maneuverability and agility of the aircraft are greatly affected. Skinner et al. [16] analyzed vortex structure in the near field of swept-tapered wings. They measured the velocity and observed the characteristics of the flow field on the wing and concluded that the breakdown is independent of the Reynolds number and has a significant dependence on the angle of attack. Kumar et al. [17] reported the nature of the vortex breakdown structure of the complicated flow field over a flying delta wing configuration with Λ=53º, Re= 3.7 × 105, and α = 25º. Their experimental observations revealed breakdown and wake-like flow on the non-slender delta wing at the mentioned angle of attack (close to the stall). One of the methods of postponing the vortex breakdown is using LEX aerodynamic surfaces [18]. Manshadi and Hashemi showed by the flow visualization that using LEX leads to the transfer of the breakdown location downstream of the diamond wing. As a result, the stall angle of the wing increases [19]. In another study, they found that the higher LEX angle produced more vortical flow [20] and created a smaller wake-like flow area behind the wing [21]. Nowadays, with the development of numerical solution codes and software, it is possible to investigate the features of vortical flow on all types of wings and the phenomenon of breakdown. Hamizi and Khan [22], by measuring the lift force and pressure on a delta wing with a Λ=70º, showed that there is a satisfactory agreement between the numerical solution and the experimental data. Boumrar and Djebali [23] showed that at α = 25º and close to the wing apex, the pressure coefficient is minimum for two cross-sections over a delta wing. They related these two areas of pressure reduction to the existence of two pairs of vortices. Manshadi et al. [24] investigated that the flow pattern on the lambda wing is highly nonlinear, which is due to the vortex breakdown at moderate and high angles of attack. Tomac and Rizzi [25] investigated that a flow field on a diamond wing at low angles of attack includes two primary and secondary separation regions. These separations are related to the formation of primary and secondary vortices. Comparing the numerical solution and the experiments revealed that the K-W SST model has a suitable prediction of the separation location of shear layers. Hashemi et al. [26] demonstrated that at a constant angle of attack, the suction-induced effect increases by shedding LEVs downstream. Yi et al. [27] showed that increasing the angle of attack in the same cross-sections leads to a higher amount of vorticity magnitude at the vortex core. However, from a specific angle, increasing the angle of attack is accompanied by a reduction in vorticity magnitude over the wing, which indicates the vortex breakdown.

Ghajar et al. [28] demonstrated that the lift coefficient (CL) and drag coefficient (CD) significantly affect aircraft performance, attributing this influence to alterations in the LEV structure with increasing angle of attack. In a subsequent investigation concerning ground effect on the flow characteristics of delta wings [29], it was observed that the lift coefficient increases with decreasing distance between the model and the ground.

The major concern regarding the numerical study of the flow field on the wing is to predict the appropriate location of vortex breakdown. For this reason, it is necessary to correct the grid study and

choose the proper turbulence model and solver. In the meantime, many studies compared the numerical solution with various experimental data, such as measuring pressure and velocity field, and flow visualization over the wing, to finally introduce the best turbulence model. Wibowo et al. [30] compared the lift coefficient and flow visualization by numerical and experimental methods (water tunnel). They concluded that the most accurate turbulence models are DES and k-ω SST with an error of less than 3%. However, in terms of solving time, the k-ω SST model is the best choice with a proper prediction of the vortex breakdown location [31].

According to the literature review performed, most of the previous research has focused on delta wing flow patterns with high leading-edge sweep-back angles. However, the identification of the flow field on the delta wing with a low leading-edge sweep-back angle and a diamond wing has received less attention. Since a diamond wing has recreated a prominent and widely used role in the design of UAVs as well as stealth fighters [32], therefore, it is novel to study the characteristics of these types of wings equipped with upstream surfaces such as LEX and a cylindrical body. The use of numerical solution software can also lead to a significant reduction in experimental costs, which is considered in the present article. The investigations carried out include the pressure coefficient over the wing, the development of the vorticity field in different sections, and the Q-criterion at α=5º, 10º, and 15º. Moreover, the measurement of the aerodynamic forces and vertical and horizontal distance of the LEV provides a suitable observation of the vortex formation and its trajectory over the wing. In this study, the vortex breakdown has been observed in which phenomenon reduces the aerodynamic performance of the wing. In the present work, the authors investigated the flow field on the diamond wing using Ansys-Fluent 18.2 software. This paper can be a suitable database for other works, especially on a diamond wing-body model equipped with LEX or a delta wing with a low sweep-back angle.

2 NUMERICAL APPROACH

The first step in the numerical solution is to design a suitable geometry and create grids. The geometry of the diamond wing, along with the body, was designed by Catia commercial software and then entered into Ansys-Fluent software (Fig. 1). The dimensions of the model are demonstrated in Table 1.

Table 1- The dimensions of the model (body and wing) along with the simulation flow conditions.

Parameter	value
Overall model span	234 mm
Wing-root chord	175 mm
Cylindrical body length	245 mm
Cylindrical body diameter	30 mm
Wing leading-edge sweep back	50º
Wing trailing-edge sweep forward	10º
Wing leading-edge angle	45º
LEX angle	16º
Re (based on overall model length)	2.16×10^5

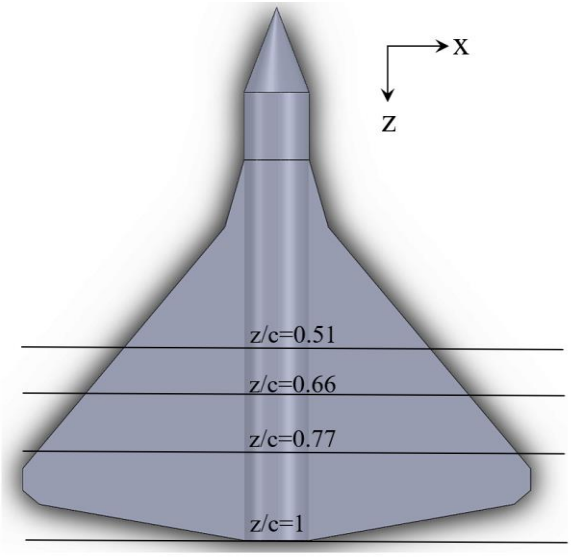

Fig. 1- The diamond wing geometry along with inestigated cross-sections.

It should be noted that the LEX with a 16º sweep angle chosen at the wing apex was selected from the previous works of the researchers [20] [26]. The governing equations include the Navier-Stokes equation and continuity. These differential equations are acquired utilizing Newton's second law of motion on a control volume. The equations

were transformed into solvable equations on the computational grids utilizing the finite-volume approach. Continuity and Navier-Stokes equations are as follows [33] [34]:

$$\frac{\partial(\rho U_i)}{\partial x_i} = 0$$

$$\frac{\partial(\rho U_i U_j)}{\partial x_j} = -\frac{\partial P}{\partial x_i} + \frac{\partial(2\mu S_{ij})}{\partial x_j} + F_i$$

In the mentioned equations, ρ is the fluid density, and U is the fluid velocity. The first term in this equation represents the rate of mass flux passing through the surface of the control volume per unit volume. In the Navier-Stokes equation, S_{ij} is the strain rate tensor, and F_i is the volume force acting on the fluid, including the forces caused by magnetic fields, which are negligible in this study. The strain rate tensor is defined as follows:

$$S_{ij} = \frac{1}{2}\left(\frac{\partial U_i}{\partial x_j} + \frac{\partial U_j}{\partial x_i}\right)$$

Continuity and Navier-Stokes equations are expressed in a general form. These equations will take different forms according to the flow conditions. The mentioned equations can be solved analytically by considering some simplifying assumptions for a laminar flow. However, in turbulent flows, these equations cannot be solved analytically, and due to the numerous complexities of the equations, mechanisms are required for numerical solutions. The k-ω SST turbulence model is used to model the turbulent flow and also to solve the Reynolds stress tensor. This model solves two additional PDEs, including a modified version of the k equation used in the k-ε model and a transport equation for ω [35]. Zhang et al. [36] revealed that there is no difference between the k-ω SST model and DES for determining the estimation of the drag force of the full-scale sedan vehicle. In this study, the free flow stream is considered 12.5 m/s, and the flow is incompressible. Thus, the pressure-based method has been used to solve equations (momentum and continuity). The k-ω SST formulation also switches to a k-ε behavior in the free-stream and thereby avoids the common k-ω problem that the model is too sensitive to the inlet free-stream turbulence properties. The k-ω SST is used for the flow field that is prone to adverse pressure gradient and separation. This turbulent model does produce a bit excessively large turbulence levels in areas with large normal strain, like stagnation regions and regions with substantial acceleration. Based on Menter [37] [38], the turbulent kinetic energy (k) and the specific dissipation (ω) are as follows:

$$\frac{\partial k}{\partial t} + U_j \frac{\partial k}{\partial x_j} = P_k - \beta^* k\omega + \frac{\partial}{\partial x_j}\left[(\vartheta + \sigma_k \vartheta_T)\frac{\partial k}{\partial x_j}\right]$$

$$\frac{\partial \omega}{\partial t} + U_j \frac{\partial \omega}{\partial x_j} = \alpha S^2 - \beta\omega^2 + \frac{\partial}{\partial x_j}\left[(\vartheta + \sigma_\omega \vartheta_T)\frac{\partial \omega}{\partial x_j}\right] + 2(1 - F_1)\sigma_{\omega 2}\frac{1}{\omega}\frac{\partial k}{\partial x_i}\frac{\partial \omega}{\partial x_i}$$

Fig. 2 demonstrates the dimensions of the solution domain along with the boundary conditions. The solution domain consists of a rectangular cube, which is 10 times the length of the wing chord from the front, top, and right side, and 20 times from the back side. This distance is determined to confirm the absence of boundary effects on the flow field around the model. The boundary conditions utilized include the inlet velocity at the inlets, the wall for the wing and cylindrical body, and the outlet pressure at the end of the domain. Furthermore, half of the wing-body model is considered for simulation because the model did not have roll and yaw maneuvers during the study. Therefore, a symmetrical boundary condition is also placed on the sidewall plane.

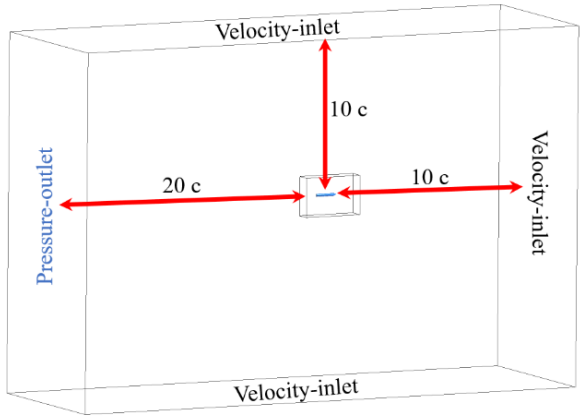

Fig. 2. Boundary conditions and domain dimensions used in the numerical solution

The governing equations are discretized in the numerical solution based on the finite volume method. Temporal and spatial discretization were performed using a second-order scheme to increase the accuracy of the results. The solver pressure-based with a SIMPLE-C [27] [37] type solution algorithm was chosen for the solution. Fig. 3 depicts the SIMPLE-C algorithm steps concerned with reaching the converged numerical solution. One of the important issues in numerical analysis is to use the minimum number of grids. The smaller the number of grids, the shorter the calculation time.

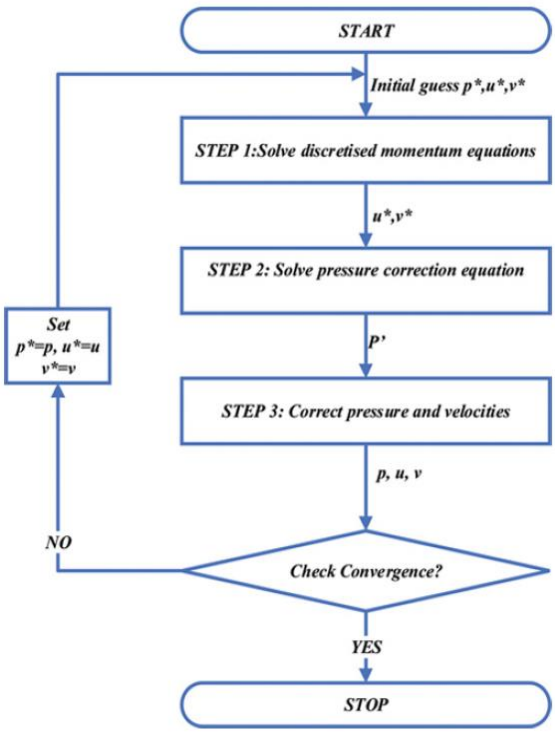

Fig. 3. Flow chart showing the SIMPLE-C algorithm [38].

However, it should be kept in mind that if there are fewer than a specific number of cells, the flow simulation results are not satisfactory [39]. Fig. 4 shows the grid independence solution at α=10º to find the most suitable number of cells. As can be seen, there are no significant changes in the normal force coefficient after the number of 4.8 million grids. Boundary layer meshing has been accomplished in order to predict the aerodynamic forces correctly. The characteristics of the boundary layer mesh, including the height of the first layer, the growth rate, and the total number of layers, are reported in Table 2.

Table 2. Characteristics of boundary layer grids

First layer height	0.000067 [m]
Growth rate	1.2
Total layers	10

Furthermore, the qualitative parameters of grids are demonstrated in Table 3. Regarding Table 3. It can be seen that the quality of the meshes is considerably satisfactory.

Table 3. The qualitative parameters of grids

Skewness	<0.89
Aspect ratio	<40
Orthogonal quality	>0.106

The number of grids (4.8 million), which are of good quality and meet the requirements of the turbulence model (y^+<4), is shown in Fig. 5.

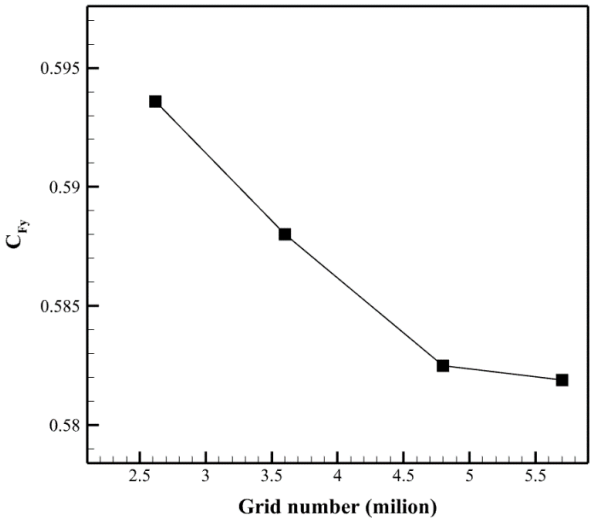

Fig. 4. The grid independence for numerical investigation.

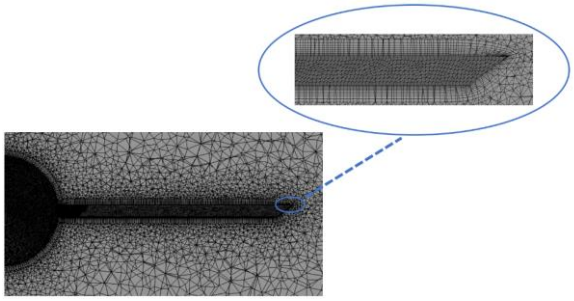

Fig. 5. A view of the grid around the model, along with the boundary layer cells.

Fig. 6 reports the convergence process of aerodynamic forces. According to it, the numerical solution results converged after 1400 iterations for solving F_y (normal force) and 500 iterations for F_z (axial force).

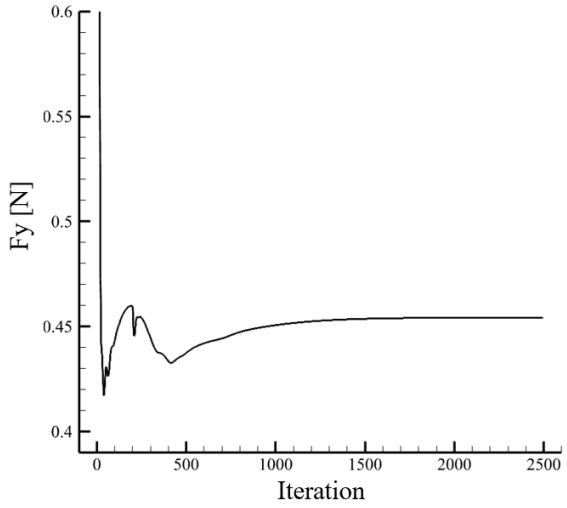

(a) Normal force

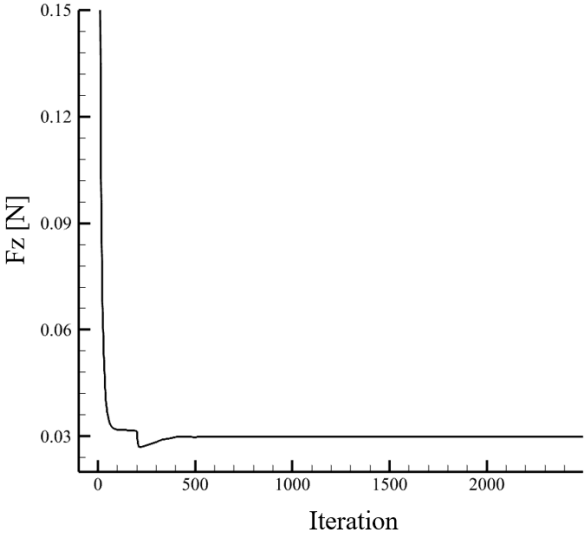

(b) Axial force

Fig. 6. The convergence process of aerodynamic forces

3 NUMERICAL VALIDATION

In order to ensure the accuracy of the results, the experimental study of Yi et al. [27] on a delta wing has been used. For this purpose, the lift coefficient was calculated at the angles of attack from 0 to 50 degrees for validation. As can be seen from Fig. 7, there is a good agreement between the present work and Ref. [27] for α=0-10º (low attack angles) degrees. A gentle difference between the results occurs from angles of 10º to 20º. After the stall angle (very high angles), the difference between the present results and experiments increases. Finally, in the last two angles, the matching of the data has become more appropriate.

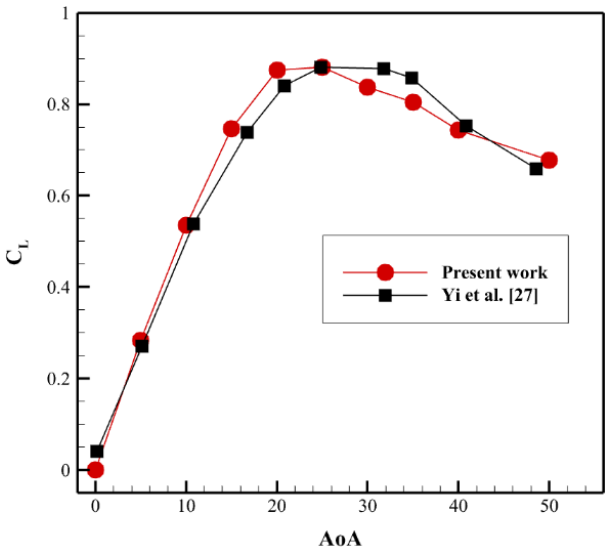

Fig. 7- Validation of the results with the research of Yi et al. [27].

4 RESULTS

In this part of the research, the numerical results are discussed for angles of attack of 5º, 10º, and 15º. These results include the analysis of the vortical flow over the diamond wing-body model at low angles of attack. For this purpose, four cross-sections have been considered, which include z/c=0.51, 0.66, 0.77, and z/c=1 (Fig. 1). Fig. 8 shows the pressure distribution over the diamond wing at α=5º and z/c=0.51, which is dimensionless relative to the free stream velocity as follows:

$$Cp = \frac{p - p_\infty}{\frac{1}{2}\rho_\infty U_\infty^2}$$

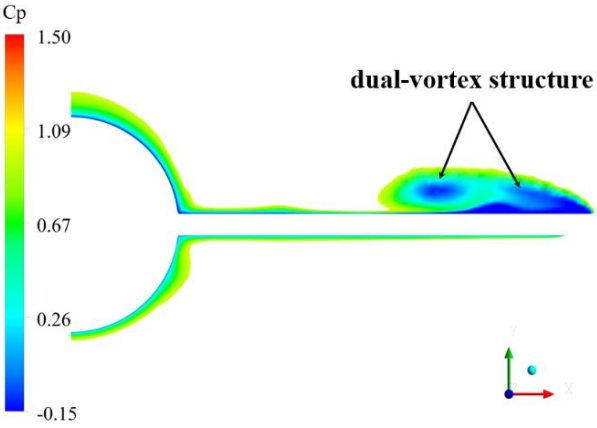

Fig. 8. Vortical flow distribution over the diamond wing at α=5º and z/c=0.51.

As can be seen, at the first span-wise cross-section, the shear layer separated from the pressure side is subjected to an adverse pressure gradient and has rolled towards the center line of the wing. In this case, a vortex structure is formed, called the leading-edge vortex (LEV). It can also be inferred that, in two areas on the wing, a sharp decrease in the pressure coefficient has occurred, which is related to the dual-structure vortex [40]. Furthermore, areas with significant weak low pressure are observed close to the model body and the wing root, which is the weak separation of the boundary layer due to the upstream surfaces (LEX and nose). Fig. 9 illustrates the distribution of the pressure coefficient on the wing's upper surface at z/c=0.51. Two areas with low-pressure coefficients are observed at y/b=0.352 and 0.414, which are related to the dual-vortex structure. The studies of previous researchers have shown that the dual-vortex structure occurs at low angles of attack over delta wings with a low sweep-back angle, lambda wings, and diamond wings [41]. In the lower part of the dual-vortex structure, a separated secondary flow is detected, which is called the secondary vortex. There is another low-pressure region close to the symmetry line of the wing (y/b=0.137). It is a very weak vortex caused by the upstream LEX surfaces. Fig. 10 plots the contour of the dimensionless pressure coefficient for the cross-section z/c=0.66 and α=5º. As can be seen, the dual-vortex structure has traveled a significant width of the wing. Actually, the shear layer under the wing (high-pressure side) has rolled towards the upper surface of the wing (low-pressure side). Rapid rotation tends to move the vortex toward the center line of the wing. In this case, the vortex diameter expanded and covered more cross-sections over the wing's suction side.

Fig. 11 shows the development of the vorticity field on the wing's upper surface at low AoAs. According to the following equation, the vorticity (stream-wise) is normalized based on the free stream velocity and the length of the wing chord:

$$\omega_z^* = \frac{\omega_z c}{U_\infty}$$

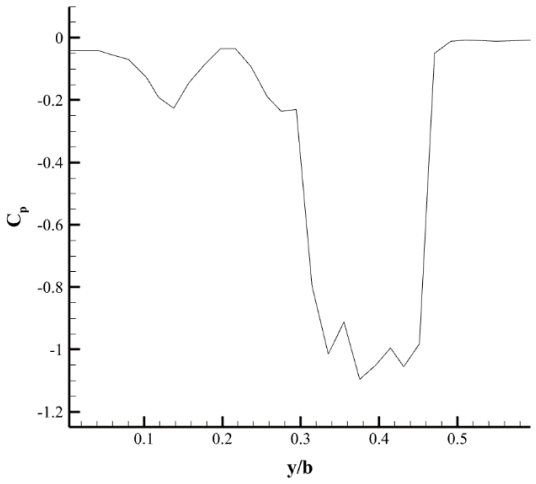

Fig. 9. Distribution of the pressure coefficient on the upper surface of the diamond wing at α=5º (z/c=0.51).

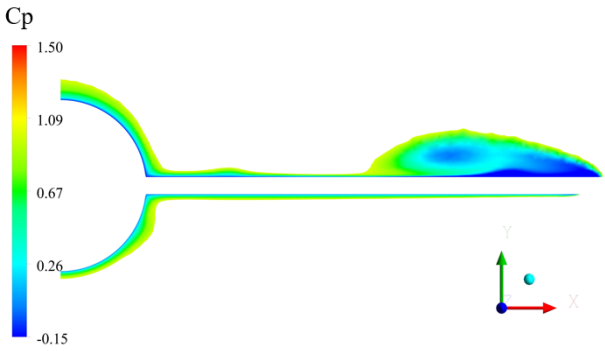

Fig. 10. Vortical flow over the diamond wing at α=5º (z/c=0.66).

For α=5º and z/c=0.51, the shear layer has moved from the pressure side to the suction side with a significant vorticity value. By comparing Figs. 8 and 11, it can be concluded that the low-pressure core of the vortex corresponds to the maximum value of vorticity. In other words, the vorticity value is very high in the low-pressure core of the vortex [41]. The shedding of LEV

towards the downstream of the wing has increased its extension towards the center line. On the other hand, for z/c=1, the shear layer separated from the leading-edge tends to reach the centerline of the wing. Due to the greater local span of the wing surface, the vortex is stretched as much as possible and covers a greater span-wise area over the upper surface. Figs. 12 and 13 depict the vertical and horizontal distance of the vortex core from the wing surface for α=5º and α=10º. The vortex core is determined by the maximum value of vorticity magnitude, and with this, the trajectory of the vortex and its diameter size can be analyzed. As can be seen, the vortex shedding downstream leads to an increase in the horizontal and vertical distance of the vortex for both angles of attack. The higher vertical distance was more severe at higher angles of attack. The remarkable point is that at α=10º, although the vortex diameter is expanded and covers more area on the wing, the horizontal trajectory is less than that compared to α=5º. On the other hand, the vortex is closer to the centerline of the wing. Considering Fig. 11, it can be obviously seen that there is another low-pressure area under the LEV with negative vorticity magnitude for both angles of attack. At α=10º, the movement of the LEV downstream and the increase in the distance between its core and the wing surface have led to the strengthening of the secondary vortex. For z/c=0.77 and α=10º (Fig. 11), the secondary vortex is typically separated from the surface. In this case, the formation of the third vortex is possible. The third vortex is small and has a positive vorticity value. Furthermore, the secondary vortex has split the structure of the LEV, and a dual-vortex structure has been created. For the last cross-section (z/c=1), the core of the vortex could not be detected, which is an indication of the breakdown in the structure of the vortices. The vortex breakdown has produced a significant area of wake-like flow behind the wing. Fig. 14 shows the Q-criteria at angles of attack of 5 and 10 degrees that are colored by the dimensionless axial velocity. Positive Q-criteria values give prominence to regions of high swirl compared to shear to represent coherent vortices [27] [34]. Considering Figs 11 and 14 (for both angles of attack), in the area close to the wing apex, a vortex flow has shed downwards at a high speed and combined with the LEV. According to the contour legend, the axial velocity of the vortex is about 1.3 times the free stream velocity. For α=10º, the formation of the secondary vortex under the LEV and dual-vortex structure is also observed. The LEV breakdown at this angle of attack is accompanied by the breakdown of the secondary vortex. Fig. 15 demonstrates the pressure coefficient and the Q-criterion for a diamond wing at α=15º. By comparing Figs. 14 and 15, it can be inferred that by increasing AoA, the axial velocity has improved. Also, the pressure coefficient at the vortex core has reduced. The vertical distance of the LEV core had an upward trend (Figs. 15 b, 8, and 10). The vortex breakdown at α=15º occurred approximately at z/c=0.77 with an increase in the pressure coefficient and a reduction of the velocity in the vortex core. However, it should be noted that the pressure coefficient gradually enhanced at this cross-section, and a low-pressure area is still observed. The shear layer is separated from the nose of the model body, which is developing downstream. Close to the body, the shear layer separated from the surface is more evident for α=15º than for α=5º and 10º.

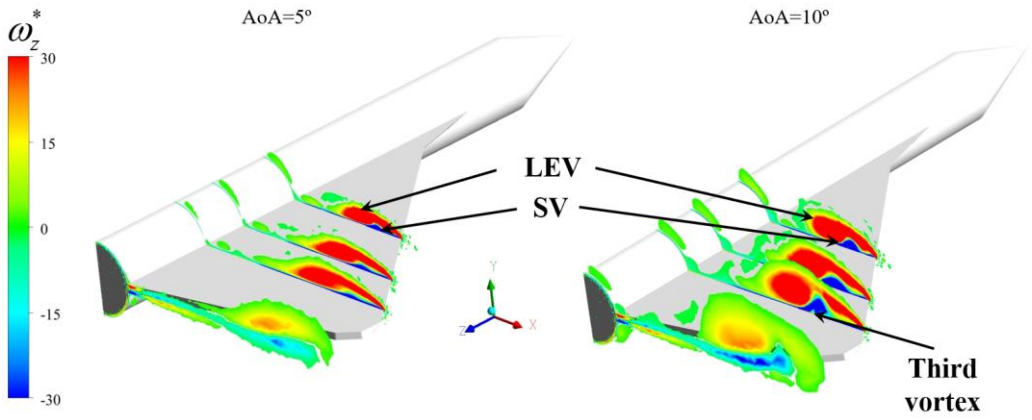

Fig. 11. Vorticity distribution over the wing (α=5º and α=10º).

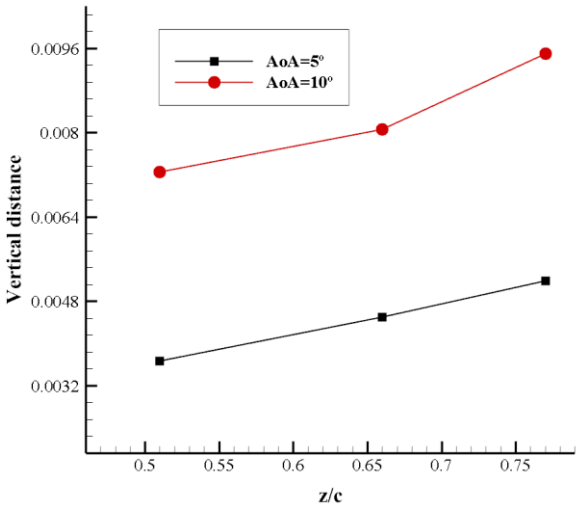

Fig. 12. The vertical distance of the vortex core from the wing surface.

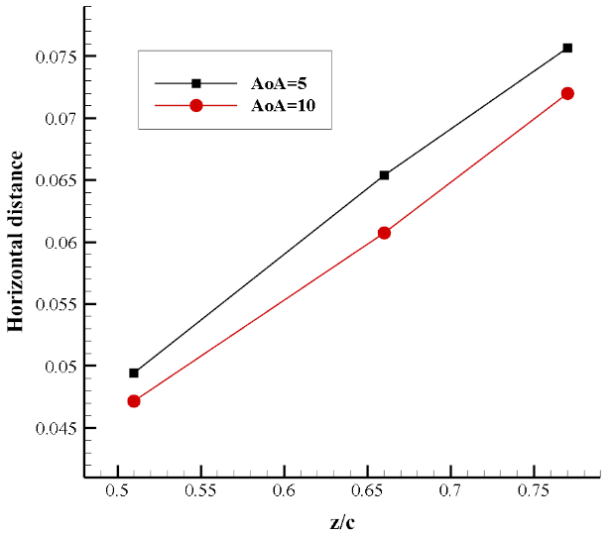

Fig. 13. The horizontal distance of the vortex core from the wing surface.

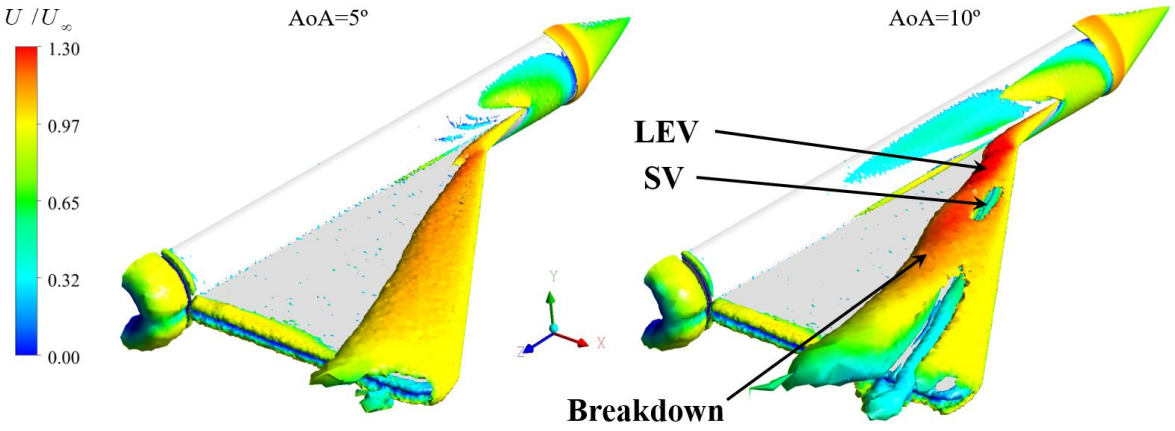

Fig. 14. Q-criteria at α=5° and α=10°.

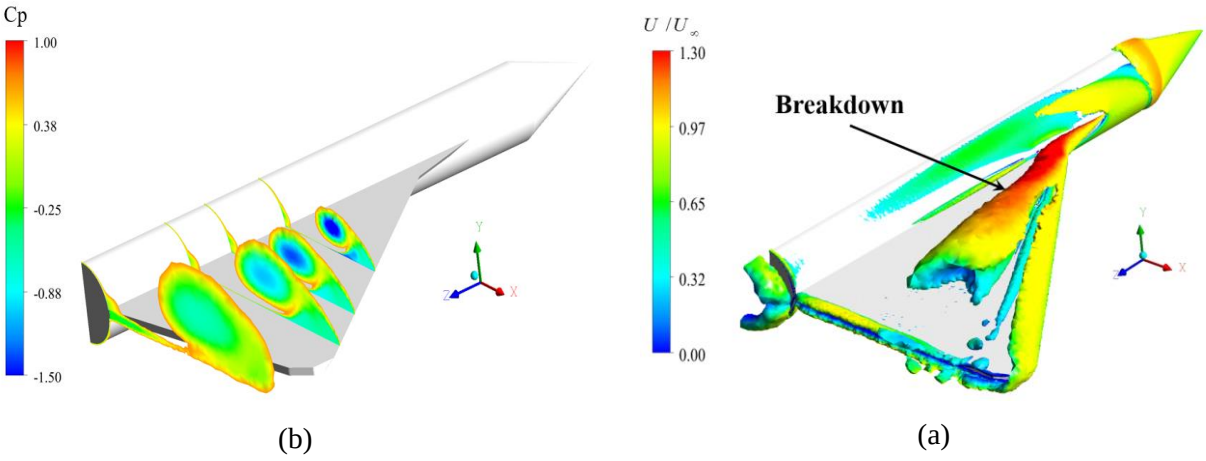

Fig. 15. Pressure coefficient and Q-criterion (α=15°).

5 AERODYNAMIC FORCE MEASUREMENTS

In this section of the article, aerodynamic forces are measured and reported in dimensionless form as follows:

$$C_L = L/0.5\rho_\infty V_\infty^2 S$$

and;

$$C_D = D/0.5\rho_\infty V_\infty^2 S$$

As illustrated in Fig. 16, increasing the angle of attack from 5° to 10° led to a sharp rise in the lift coefficient. For 10°<α<15°, CL continued to improve; however, the rate of increase was lower compared to the previous interval. A growth in the drag coefficient is also observed for the investigated model within the angle of attack range of 5° to 15°, with a notably steeper rise in CD appearing in the range of 5°<α<10°.

Fig. 17 presents the lift-to-drag ratio (CL/CD), which serves as a measurement of aerodynamic efficiency. As shown in Fig. 17, increasing the angle of attack from 5° to 10° results in a notable decline in the CL/CD ratio, with a reduction of approximately 17.1% observed at α=10°. According to the findings of Shams-Taleghani and Ghajar [42], this sharp decrease is attributed to increased drag resulting from vortex breakdown. Finally, the CL/CD curve exhibits a mild upward trend within the angle of attack range of 10°< α <15°.

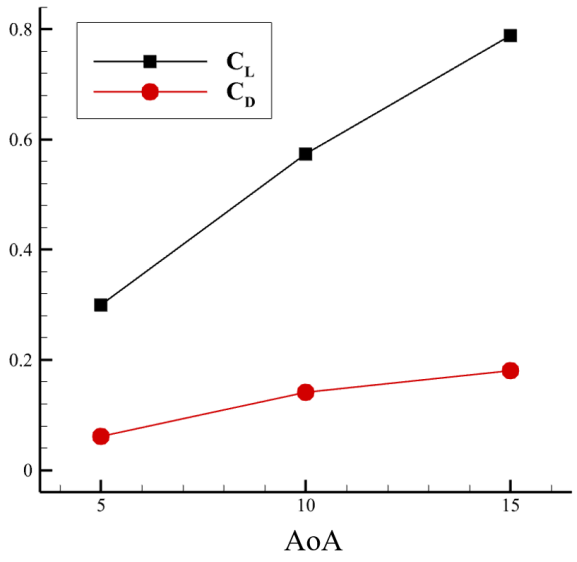

Fig. 16. Variation of aerodynamic coefficients with AoA

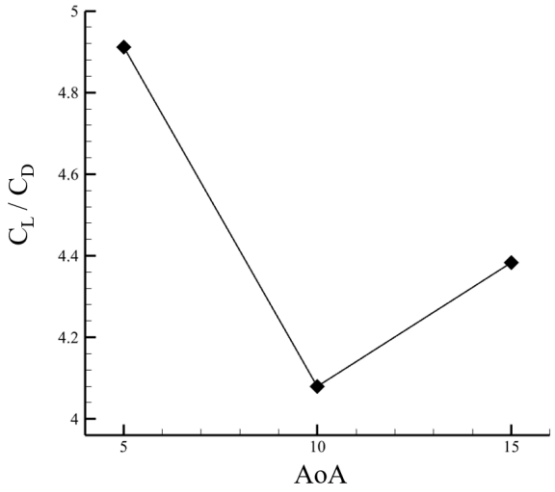

Fig. 17. Variation of CL/CD with AoA

6 CONCLUSION

In this article, the flow around a diamond wing at low angles of attack has been studied. For this purpose, numerical solution software is used for angles of attack of 5º, 10º, and 15º. Studying the flow field for this type of wing (diamond and non-slender delta wing) can help to identify the vortical flow, especially the phenomenon of vortex breakdown. The investigated diamond wing has a chord and span of 175 and 234 mm, respectively, attached to a cylindrical body with a length of 245 mm. During the flow simulation, the Reynolds number was considered equal to 2.16×10^5 (based on the model length). The results obtained are as follows:

1) For α=5º and cross-section z/c=0.51, the shear layer separated from the apex forms a coherent LEV.
2) Downstream of the wing, the LEV core expanded, and a secondary vortex was formed close to the wing surface. The secondary vortex breaks the LEV, forming a double-vortex structure.
3) An increase in the angle of attack has led to the enhancement of the LEV vorticity value and reduced the horizontal distance. It means that at a higher AoA, the vortex stretches toward the wing symmetry line.
4) For α=10º and z/c=0.77, a third vortex is formed under the secondary vortex..
5) For angles of attack of 5 and 10 degrees, the vortex breakdown occurred at z/c=1, which

was revealed by the existence of wake-like flow, pressure growth, and a fall in velocity at the vortex core.

6) The pressure coefficient increased gently from cross-sections z/x=0.66 to z/c=0.77 (α=15º).

NOMENCLATURE

Re	Reynolds number	C_{Fy}	Normal force coefficient
BWB	Blended Wing Body	P_∞	Free stream pressure
LEV	Leading-edge Vortex	ρ_∞	Free stream density
LEX	Leading-edge Extension	U_∞	Free stream velocity
α	Angle of attack (AoA)	b	Semi-span
Cp	Pressure coefficient	x	Span-wise direction
Λ	Sweep-back angle	y	Normal direction
y^+	Dimensionless first grid cell	z	Stream-wise direction
SV	Secondary Vortex	ω_z	Stream-wise vorticity
c	Wing span	C_D	Coefficient of Drag
C_L	Coefficient of lift		

HIGHLIGHTS

1. Vortical flow investigation over a low sweep-back diamond wing equipped with LEX
2. CFD carried out at α= 5º, 10º, and 15º, and Re= 2.16×10^5 based on the model length
3. As AoA increases, the vortex core extends and stretches toward the wing symmetry line.

At high AoA, a third vortex is formed under the secondary vortex, which enhances the local wing circulation.

CONFLICT OF INTEREST

No potential conflict of interest was reported by the authors.

REFERENCES

[1] L. WANG, B. SONG, Zh. Ch. SUN, and X. YANG. "Review on ultra-lightweight flapping-wing nano air vehicles: Artificial muscles, flight control mechanism, and biomimetic wings." *Chinese Journal of Aeronautics*, vol. 36, no.6, 2023, pp. 63-91, https://doi.org/10.1016/j.cja.2023.03.031.

[2] Voß, Arne. "Design and structural optimization of a flying wing of low aspect ratio based on flight loads." PhD Thesis., Technische Universität Berlin, 2020, https://doi.org/10.14279/depositonce-9858.

[3] E. Sepulveda, and H. Smith. "Technology challenges of stealth unmanned combat aerial vehicles." *The Aeronautical Journal*, vol. 121, (1243), 2017, pp. 1261-1295, https://doi.org/10.1017/aer.2017.53.

[4] E. Sepulveda, H. Smith, and D. Sziroczak "Multidisciplinary analysis of subsonic stealth unmanned combat aerial vehicles." *CEAS Aeronautical Journal*, vol. 10, no. 2, 2019, pp. 431-442,https://doi.org/10.1007/s13272-018-0325-0

[5] Xia, Xi, and Kamran Mohseni. "A theory on leading-edge vortex stabilization by span-wise flow." *Journal of Fluid Mechanics*, vol. 970 2023, https://doi.org/10.1017/jfm.2023.613.

[6] Muir, Rowan Eveline, Abel Arredondo-Galeana, and Ignazio Maria Viola. "The leading-edge vortex of swift wing-shaped delta wings." *Royal Society Open Science*, vol. 4, no. 8, Art. No. 170077, 2017, https://doi.org/10.1098/rsos.170077.

[7] Ol, Michael V., and Morteza Gharib. "Leading-edge vortex structure of non-slender delta wings at low Reynolds number." *AIAA journal*, vol. 41, no. 1, 2003, pp. 16-26, https://doi.org/10.2514/2.1930.

[8] Butler, Ethan. "Delta Wing Leading-Edge Vortex Control Using Active Flow Control Jets." PhD diss., The Ohio State University 2024.

[9] M. Werner, A. Schütte, and S. Weiss. "Turbulence Model Effects on Vortex Interaction Prediction on a Multiswept Delta Wing." *Journal of Aircraft*, vol. 61, no. 1, 2024, pp. 211-221, https://doi.org/10.2514/1.C037421.

[10] V. Kumar, A. C. Mandal, and K. Poddar. "An experimental investigation on the aerodynamic characteristics and vortex dynamics of a flying wing." *The Aeronautical Journal*, vol. 128, 2024, pp. 1-25, https://doi.org/10.1017/aer.2023.115.

[11] J. Tan, Zhijin Wang, and Ismet Gursul. "Post-stall flow control on aerofoils by leading-edge flags." *Journal of Fluid Mechanics*, vol. 972 , 2023, https://doi.org/10.1017/jfm.2023.

[12] A. Srour, H. Noura, and S. El Assaad. "Modeling, design, and manufacturing of delta-wing UAV." *In 2021 International Conference on Unmanned*

Aircraft Systems (ICUAS), 2021, pp. 1573-1579, 10.1109/ICUAS51884.2021.9476885.

[13] Pfnür, Stefan, Jonathan Pflüger, and Christian Breitsamter. "Analysis of vortex flow phenomena on generic delta wing platforms at subsonic speeds." In New Results in Numerical and Experimental Fluid Mechanics XII: Contributions to the 21st STAB/DGLR Symposium, Darmstadt, Germany, 2018, pp. 328-337. Springer International Publishing, 2020, https://doi.org/10.1007/978-3-030-25253-3_30.

[14] Landa, Tim, Lorenz Klug, Rolf Radespiel, Silvia Probst, and Tobias Knopp. "Experimental and numerical analysis of a stream-wise vortex downstream of a delta wing." *AIAA Journal*, vol. 58, no. 7, 2020, pp. 2857-2868, https://doi.org/10.2514/1.J058650.

[15] Pashilkar, A. A. "Surface pressure model for simple delta wings at high angles of attack." *Sadhana*, vol. 26, 2001, pp. 495-515, https://doi.org/10.1007/BF02703456.

[16] S. N. Skinner, R. B. Green, and H. Zare-Behtash. "Wingtip vortex structure in the near-field of swept-tapered wings." *Physics of Fluids*, vol. 32, no. 9, 2020, https://doi.org/10.1063/5.0016353.

[17] V. Kumar, A. C. Mandal, and K. Poddar. "Experimental study of vortex breakdown over a nonslender flying wing at high angle of attack." *In Aiaa Aviation 2021 Forum*, pp. 2609, 2021, https://doi.org/10.2514/6.2021-2609.

[18] Chou, Moo-Ting, Jiun-Jih Miau, and Li-Yu Chen. "Vortex interaction on a LEX configuration." *Journal of Visualization*, vol. 24, no. 6, 2021, pp. 1189-1205,https://doi.org/10.1007/s12650-021-00764-0.

[19] M. R. Hashemi, and M. Dehghan Manshadi, "Experimental Study of LEX Angle Effect on Vortical Flow Over the Diamond Wing with Airfoil-Shaped Section by Using Hot-wire and Five-hole Probe." Journal of Solid and Fluid Mechanics, vol. 12, no. 2, 2022, pp. 81-91, https://doi.org/10.22044/JSFM.2022.9578.3164.

[20] M. R Hashemi and M. Dehghan Manshadi. "Experimental study of the effect of the LEX angle on the flow pattern of a diamond wing with an airfoil cross-section." *Journal of Visualization*, vol. 26, no. 6, 2023, pp. 1247-1262, https://doi.org/10.1007/s12650-023-00942-2.

[21] M. Dehghan Manshadi, M. R. Hashemi, and M. Ilbeigi. "The evaluation of the angle of attack effects on the structure of the diamond wing with the sharp leading edge being equipped with LEX by using flow visualization." Journal of Solid and Fluid Mechanics, vol. 9, no. 3, 2019, pp. 265-275, https://doi.org/10.22044/JSFM.2019.8618.2960.

[22] Hamizi, Ilya Bashiera, and Sher Afghan Khan. "Aerodynamics investigation of delta wing at low Reynolds' number." CFD Letters, vol. 11, no 2, 2019, pp. 32-41.

[23] I. Boumrar and R. Djebali., "Experimental validation of pressure distribution prediction under delta wing apex vortex at high Reynolds numbers." CFD *Letters*, vol. 11, no. 3, 2019, pp. 92-102.

[24] M. Dehghan Manshadi, M. Eilbeigi, M.Kazem Sobhani, M. Bazaz Zadeh, and M. A. Vaziry, "Experimental study of flow field distribution over a generic cranked double delta wing." *Chinese Journal of Aeronautics*, vol. 29, no. 5, 2016, pp. 1196-1204, https://doi.org/10.1016/j.cja.2016.08.002.

[25] M. M., Tomac, and A. W. Rizzi. "CFD study of vortex separation phenomena on the blunt diamond wing." *In 53rd AIAA Aerospace Sciences Meeting*, 2015, pp. 0291, https://doi.org/10.2514/6.2015-0291.

[26] M. R. Hashemi, S. M. Malek Jafarian, and M. Dehghan Manshadi, "Experimental investigation of vortical flow induced by canard on a diamond wing equipped with LEX." *Journal of Aerospace Science and Technology*, vol. 17, no. 1, 2024, pp. 90-100, 10.22034/jast.2023.417448.1160.

[27] Y.Yi, T. Hu, P. Liu, Q. Qu, G. Eitelberg, and R.AD Akkermans. "Dynamic lift characteristics of a nonslender delta wing in large-amplitude pitching." *Aerospace Science and Technology*, vol. 105, Art. No. 105937, 2020, https://doi.org/10.1016/j.ast.2020.105937.

[28] S. A. Shams Taleghani, A. Ghjar, M. R. Soltani, and M. Masdari, "Experimental investigation of ground effects on aerodynamic characteristics of a delta wing airplane model" *Modares Mechanical Engineering*, vol. 17, no. 9, 2017.

[29] A. Ghajar, S. A. Shamstaleghani, M. R. Soltani, and M. Masdari. "Experimental investigation of angle of attack effects on aerodynamic characteristics of delta wing-body-vertical tail combination airplane model in ground effects." 2020, pp: 143-151.

[30] Wibowo, Setyawan Bekti, and Tri Agung Rohmat. "An evaluation of turbulence model for vortex breakdown detection over a delta wing." *Archive of Mechanical Engineering*, vol. 65, no. 3, 2018, https://doi.org/10.24425/124489.

[31] B. Shahriari and M. R. Hashemi. "Numerical solution of hovering propeller performance at various blade pitch angles and revolutions with different turbulence models." *Journal of Simulation and Analysis of Novel Technologies in Mechanical Engineering*, vol. 15, no. 4, 2023, pp. 5-15,

[32] D. Bacci and I. Vagias. "A trade-off analysis between lateral/directional stability and radar cross section requirements of an air-to-air combat airframe." *Aerospace Science and Technology*, vol.

138, Art. no. 108361, 2023, https://doi.org/10.1016/j.ast.2023.108361.

[33] Sh. M. Beigi, A. Shateri, and M. Dehghan. Manshadi. "Numerical investigation of the effect of the location of stern planes on submarine wake flow." Ocean Syst Eng 10, no. 3, 2020, pp. 289-316, https://doi.org/10.12989/ose.2020.10.3.289.

[34] M. R., Hashemi, P. Hashemi, and M. Dehghan Manshadi. "The Effects of Sweep-Back Angle on Dynamic Lift Characteristics of Delta Wing During Large-Amplitude Pitching." *International Journal of Aeronautical and Space Sciences*, vol. 26, 2025, pp. 1-16, https://doi.org/10.1007/s42405-024-00878-3

[35] D. C. Wilcox, *Turbulence modeling for CFD*. vol. 2. La Canada, CA: DCW industries, 1998.

[36] Ch. Zhang, , Ch. Patrick Bounds, L. Foster, and M. Uddin. "Turbulence modeling effects on the CFD predictions of flow over a detailed full-scale sedan vehicle." *Fluids*, vol. 4, no. 3, 2019, https://doi.org/10.3390/fluids4030148.

[37] Q. Chen, T. Hu, P. Liu, Q. Qu, H. Guo, and R. AD Akkermans. "The dynamic vortical flow behavior on a coplanar canard configuration during large-amplitude pitching." *Aerospace Science and Technology*, vol. 112, 2021, Art. no. 106553, https://doi.org/10.1016/j.ast.2021.106553.

[38] R. Abed Mahdi, H. A. Mohammed, K. M. Munisamy, and N. H. Saeid. "Experimental and numerical investigation of combined convection heat transfer and fluid flow around a circular cylinder through rectangular and trapezoidal Open-Cell aluminum foams." *Chemical Engineering Communications*, vol. 202, no. 5, 2015, pp. 674-693, https://doi.org/10.1080/00986445.2013.863188.

[39] Xiang IA. Yang, , and K. P. Griffin. "Grid-point and time-step requirements for direct numerical simulation and large-eddy simulation." *Physics of Fluids*, vol. 33, no. 1, 2021, https://doi.org/10.1063/5.0036515.

[40] Murat Yavuz, M. "Investigation of flow characteristics and vortex formations of the lambda wing at high angles of attack." *Journal of Thermal Engineering*, vol. 6, no. 6, 2020, pp. 282-297, https://doi.org/10.18186/thermal.829872

[41] Chen, Long, Bo Cheng, and Jianghao Wu. "Vorticity dynamics and stability of the leading-edge vortex on revolving wings." *Physics of Fluids*, vol. 35, no. 9, 2023, https://doi.org/10.1063/5.0160346.

[42] A. Shams Taleghani and A. Ghajar. "Aerodynamic characteristics of a delta wing aircraft under ground effect." *Frontiers in Mechanical Engineering*, vol. 10, 2024, https://doi.org/10.3389/fmech.2024.1355711.

HOW TO CITE THIS ATRICLE

F. Author, S. Author, and T. Author, "Numerical Study of Flow Pattern on A Diamond Wing-Body Equipped with LEX At Low Angles of Attack," *Journal of Aerospace Science and Technology*, Vol. 18, Issue 2, 2025, pp. 75-87

DOI: https://doi.org/10.22034/jast.2025.473495.1204

URL: https://jast.ias.ir/article_224358.html